MOLECULAR REPRODUCTION AND DEVELOPMENT 74:116–124 (2007)

RNA Interference as a Tool to Study the Function of MAD2 in Mouse Oocyte Meiotic Maturation

JIAN-YING WANG,[1,2] ZI-LI LEI,[2] CHANG-LONG NAN,[2] SHEN YIN,[2]
JINGHE LIU,[2] YI HOU,[2] YUN-LONG LI,[1] DA-YUAN CHEN,[2] AND QING-YUAN SUN[2]*

[1]*Key Laboratory of Animal Resistance Research, College of Life Science, Shandong Normal University, Jinan, P.R. China*
[2]*State Key Laboratory of Reproductive Biology, Institute of Zoology, Chinese Academy of Sciences, Beijing, P.R. China*

ABSTRACT Spindle checkpoint proteins control entry into anaphase and chromosome segregation. As a member of spindle checkpoint proteins, MAD2 takes a central role in the regulation of anaphase onset and genome integrity. Here, we used MAD2 siRNA transfection approach to study MAD2 functions during mouse oocyte meiotic maturation in vitro. Real-time PCR and laser scanning confocal microscopy showed that we successfully downregulated MAD2 transcript and protein expression. We further demonstrated that MAD2 downregulation resulted in a shortened duration of meiosis I and meiotic spindle abnormality, suggesting the function of MAD2 in mouse oocyte meiotic maturation. We also showed that MAD2 interference to some extent decreased GVBD rate, but increased apoptosis in mouse oocytes. In conclusion, our study shows that siRNA transfection is an effective tool to study MAD2 functions, and our results provide further evidence for the role of MAD2 as a spindle checkpoint protein in mouse oocytes. *Mol. Reprod. Dev. 74: 116–124, 2007.* © 2006 Wiley-Liss, Inc.

Key Words: RNA interference; MAD2; mouse oocyte; meiosis; checkpoint

INTRODUCTION

Mammalian oocytes are arrested at the diplotene stage of the first meiotic prophase, which is also termed the germinal vesicle (GV) stage. The prophase-I-arrested state is described as immature, and the process of first meiosis resumption and completion is called meiotic maturation. The resumption of meiotic maturation is manifested by germinal vesicle breakdown (GVBD), followed by chromatin condensation and microtubule reorganization. These events lead to the formation of a metaphase spindle and subsequent completion of the first meiotic division, after which oocytes enter the second meiosis and become arrested at metaphase II (MII) until fertilization or parthenogenetic activation.

Segregation of sister chromatids or homologous chromosomes during anaphase is a key event in both mitosis and meiosis. Any error in this process may cause aneuploidy. To avoid these errors, both mitotic and meiotic cells have evolved a surveillance mechanism, the spindle checkpoint to detect the attachment of sister chromatids or homologous chromosomes to microtubules. This spindle checkpoint is able to detect a single, unaligned chromosome in the spindle and arrest the cell cycle at metaphase to allow more time for all the chromosomes to move into the correct orientation at the spindle equator before the chromosomes separate (Musacchio and Hardwick, 2002; Wang and Sun, 2006). The spindle checkpoint inhibits the ubiquitin ligase activity of the anaphase-promoting complex or cyclosome (APC/C), thus preventing precocious chromosome segregation and ensuring the accurate partition of the genetic material (Bharadwaj and Yu, 2004). Spindle assembly checkpoint proteins including Mad1, Mad2, MAD3/BubR1, Bub1, Bub3, and Mps1 control entry into anaphase and chromosome segregation, and loss of these proteins may induce genomic instability and cancer.

Wassmann et al. (2003) for the first time showed that a functional Mad2-dependent spindle checkpoint existed during the first meiotic division in mammalian oocytes. Our recent studies showed that MAD2 is also a meiotic spindle checkpoint protein in rat oocytes (Zhang et al., 2004). MAD2 exists at the kinetochores at GV and prometaphase I stages; once the metaphase I spindle is formed and all chromosomes are aligned at the equator of the spindle, MAD2 is released into the cytoplasm. A recent study further demonstrated that Mad2 is required for inhibiting securin and cyclin B degradation following spindle depolymerization in meiosis I mouse oocytes (Homer et al., 2005a). Another recent report showed that injection of Capped hMad2–GFP mRNA into the mouse oocytes increased incidence of aneuploidy and shortened duration of meiosis I, while

Grant sponsor: National Natural Science Foundation of China; Grant numbers: 30430530, 30225010, 30570944; Grant sponsor: Special Funds for Major State Basic Research Project of China.

*Correspondence to: Prof. Qing-Yuan Sun, State Key Laboratory of Reproductive Biology, Institute of Zoology, Chinese Academy of Sciences, #25 Beisihuanxi Rd., Haidian, Beijing 100080, China.
E-mail: sunqy1@yahoo.com or sunqy@ioz.ac.cn

Received 25 February 2006; Accepted 15 April 2006
Published online 21 August 2006 in Wiley InterScience (www.interscience.wiley.com).
DOI 10.1002/mrd.20552

TABLE 1. Primer Sequences of β-Actin and *MAD2* for Real-Time PCR and Plasmid Construction

Genes	Accession number	Primer sequences (5′–3′)		PCR product length (bp)
Mouse *MAD2*	NM019499	TCAGCGTGGCATTTATCC	ATTGCGGTCCCGATTCTT	422
Mouse β-actin	X03672	CCCTAAGGCCAACCGTGAA	CAGCCTGGATGGCTACGTACA	83

overexpression of Mad2 inhibited homolog disjunction (Homer et al., 2005b). Our recent work proved that reduced expression of MAD2 was correlated with missegregation of chromosomes and decreased BCL2 (an anti-apoptosis protein) expression as well as aggregation of mitochondria (a trait of oocyte aging) (Ma et al., 2005).

The present study aims to further investigate the role of MAD2 during mouse oocyte meiotic maturation using another alternative of RNAi approach, siRNA transfection, paying attention particularly to the effect of MAD2 downregulation on oocyte meiosis resumption, chromosome alignment, meiotic apparatus morphology, and apoptosis.

MATERIALS AND METHODS

Reagents and Antibodies

MAD2 siRNA (sc-35838), control siRNA (sc-37007), and fluorescein conjugate control siRNA (sc-36869) were purchased from Santa Cruz Biotechnology, Inc. (Santa Cruz, CA) *TaKaRa Ex Taq*™ R-PCR Ver.2.1 (DRR031A), mRNA selective PCR kit Ver.1.1 (Code DRR025A), and pMD 18-T Vector (Code D504A)were purchased from Takara Biotechnology Dalian Co. Ltd. (Dalian, China) SYTO® 11 green fluorescent nucleic acid stain (Code S7573), Opti-MEM I reduced-serum medium (Code 31985-070), Trizol (Code 15596-026), Lipofectamine 2000 (Code 11668-027), Leibovitz's L-15 tissue culture medium (Code 11415-064) were purchased from Invitrogen Corporation (Carlsbad, CA). SYBR Green I Nucleic Acid Gel Stain (Code J976) was purchased from AMRESCO, Inc. (Solon, OH). MAD_2 polyclonal antibody (PRB-452C) was purchased from Jingmei Biotech Co., Ltd. Monoclonal FITC-anti-tubulin antibody derived from mouse and all the other chemicals used in this study were purchased from Sigma Chemical Company (St. Louis, MO). Programmed cell death detection kit was purchased from Dingguo Biotechnology Co. (Beijing, China).

Oocyte Collection

Animal care and handling were conducted in accordance with policies regarding the care and use of animals promulgated by the ethical committee of the Institute of Zoology, Chinese Academy of Sciences. The oocytes were collected from Kunming white mice, a native breed widely used in biological research in China. GV-stage oocytes were collected from ovaries of 4- to 6-week-old female mice at 48 h after pregnant mare's serum gonadotropin treatment. Cumulus-enclosed GV oocytes were collected by puncturing the large antral follicles with a needle in Leibovitz L-15 tissue culture medium containing 10% fetal bovine serum. The cumulus cell masses surrounding the oocytes were removed by repeated pipetting before culture and treatment.

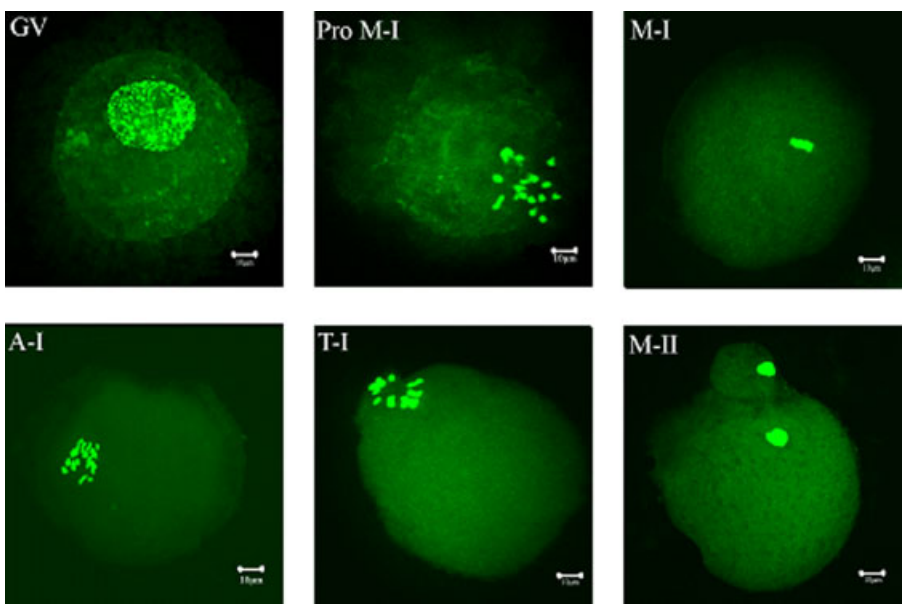

Fig. 1. Typical images of oocyte at various maturation stages. [See color version online at www.interscience.wiley.com.]

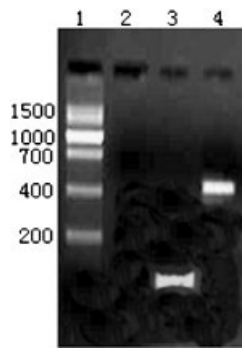

Fig. 2. PCR amplification of mouse MAD2 and β-actin gene. Amplification of 422 bp and 83 bp fragments of the mouse MAD2 and actin gene were presented in the Figure. Lane 1, 200-bp Ladder size marker; lane 2, no template control; lane 3, amplification product of β-actin (83 bp).; lane 4, amplification product of MAD2 (422 bp).

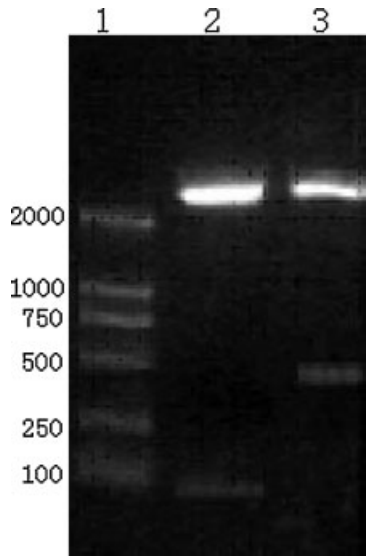

Fig. 4. Identification of mouse MAD2 and β-actin by endonuclease digestion. Lane1, Takara DL2000 marker; lane 2, mouse pMD18T-β-actin; lane 3, mouse pMD18T-MAD2.

siRNA Transfection

For siRNA transfection, the procedures were basically the same as reported previously (Lazar et al., 2004). The zona pellucida (ZP) was removed by incubation in acid Tyrode's solution (pH = 2.5) for a few seconds, followed by several washes in a large volume of L-15 tissue culture medium. Meiotically arrested oocytes, incubated in the presence of IBMX (20 μM), were transfected by MAD2 siRNA (10 μM), using lipofectamine 2000 (35 μg/ml). Control siRNA was employed to generate the control oocytes. After 7 hr, the oocytes were transferred to different media for different treatments and numbered as 0 hr time point. Apoptosis test and real time PCR were conducted at this time. For the study of the effect on meiotic maturation, the oocytes were transferred to an inhibitor-free medium for an additional incubation time in a humidified 5% CO_2 incubator at 37°C. Other oocytes were transferred to an inhibited medium with none transfection reagents for additional incubation time and then subjected to immunofluorescence staining. These oocytes were examined morphologically for the presence of GV with a StereoZoom microscope.

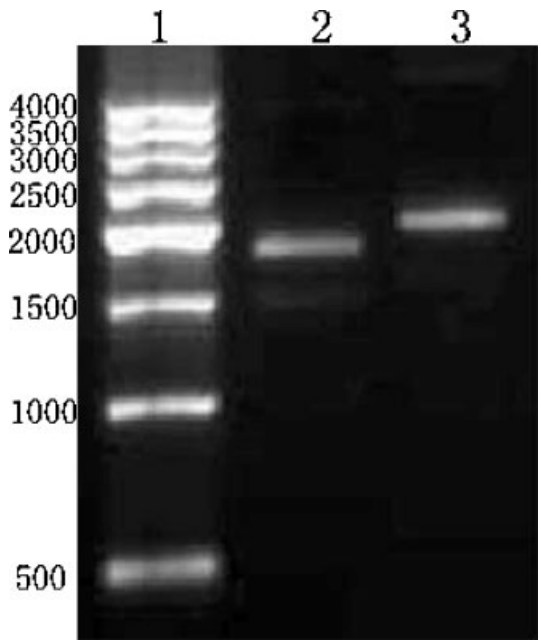

Fig. 3. Detection of plasmids. Lane 1, 500-bp ladder size marker; lane 2, mouse pMD18T-β-actin; lane 3, mouse pMD18T-MAD2.

RNA Isolation and Two Step Real-Time PCR

RNA isolation. The RNA was isolated from about 200 mouse oocytes. Extraction of RNA was performed using Trizol (Invitrogen) in accordance to the manufacturer's protocol. Total RNA was dissolved in DEPC-treated ultrapure water, and quantified by means of UV-spectrophotometry. The purity was assessed by nucleic acid/protein ratio at OD260/OD280. The ratio OD260/OD280 > 1.80 was obtained for all samples.

Reverse transcription. First strand complementary DNA was synthesized by priming with oligo dT primer as per mRNA selective PCR kit protocol. Reverse transcription was performed at 42°C for 30 min by addition of 10 μl 2°C 2× mRNA selective PCR buffer I or II, 4 μl $MgCl_2$, 2 μl dNTP/analog mixture, 0.4 μl RNase inhibitor, 0.4 μl AMV RTase XL, 0.4 μl oligo dT primer, 1 μl template, and 1.8 μl RNase free dH_2O in a final volume of 20 μl, after cooling to room temperature.

Primer design. Complementary DNA PCR primers were designed using Oligo primer analysis software (National Biosciences, Inc., Plymouth, MN) from DNA and RNA sequences obtained from GenBank for mouse *MAD2* (Accession number NM019499) and β-actin (X03672). The primers were synthesized by Takara Biotechnology Dalian Co. Ltd. (Dalian, China). Primer sequences are presented in Table 1.

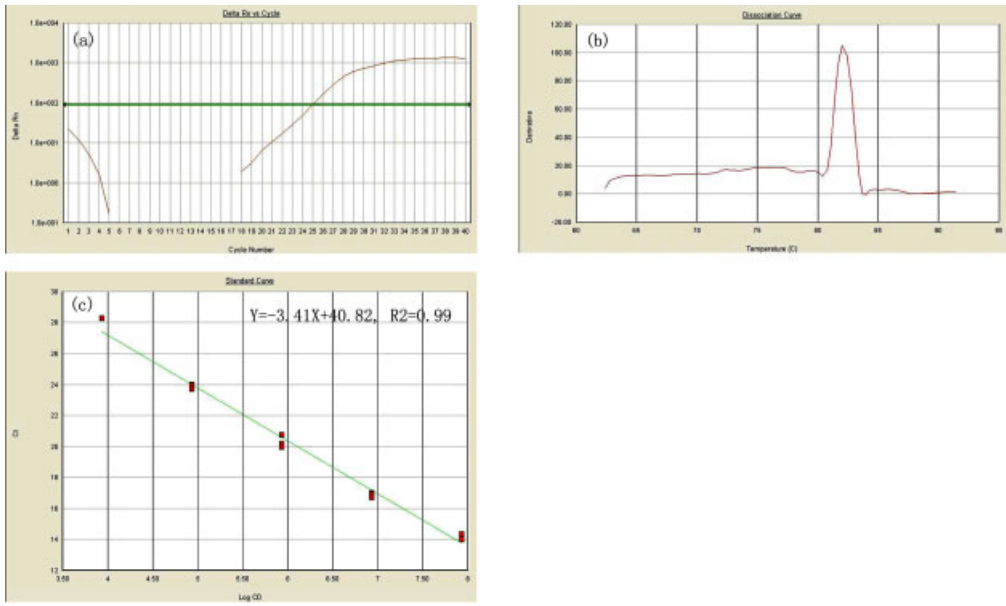

Fig. 5. Amplification curve (**a**), melting curve (**b**), and standard curve (**c**) of mouse MAD2 mRNA amplified by real-time PCR. [See color version online at www. interscience.wiley.com.]

Real-time PCR. Following reverse transcription, 1 μl of cDNA was made in 25 μl final reaction volume by qPCR in a 96-well optical PCR plate using Applied Biosystems 7000 real-time PCR system. qPCR was performed using the manufacturer's recommended conditions and dissociation curves were typically generated post-run using SDS Software (version 3.5: Roche). Standard curves were generated. After analysis, the target gene expression was normalized to beta-actin. Following PCR, the results table was exported to Excel (Microsoft Corp., Redmond, WA), and quantitative analysis for samples was regressed from the raw data. The reaction mixture consisted of 5 μl 5 × real time PCR buffer (Mg^{2+}-free), 0.75 μl dNTP mixture (10 mM), 0.5 μl Mg^{2+} solution (250 mM), 0.25 μl *TaKaRa Ex Taq* HS (5 U/μl), 1 μl template (<30 ng), 1.25 μl SYBR Green I (20×), 0.5 μl forward primer (50 μM), 0.5 μl reverse primer (50 μM), and dH_2O up to 25 μl. The PCR

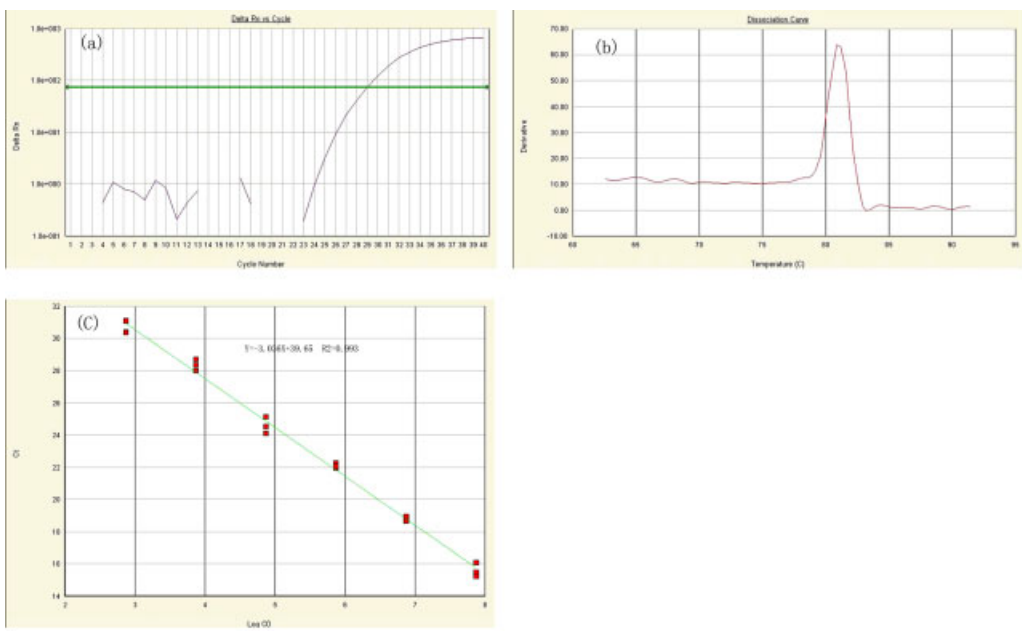

Fig. 6. Amplification curve (**a**), melting curve (**b**), and standard curve (**c**) of mouse β-actin mRNA amplified by real-time PCR. [See color version online at www. interscience.wiley.com.]

TABLE 2. Ct Value of MAD2 and β-Actin Gene Expression at Various Stages of Maturation as Determined by QPCR Analysis (means ± SD)

	GV	Pro M-I	MI	MII
β-actin	29.96 ± 0.095	28.87 ± 0.187	27.54 ± 0.482	29.9 ± 0.735
Mad2	29.63 ± 0.455	26.99 ± 0.019	25.67 ± 0.411	27.16 ± 0.105

procedure started with 50°C for 2 min to activate UNG, and the basic protocol for real-time PCR was an initial incubation at 95°C for 10 min to activate modified Taq polymerase. Forty cycles of PCR were carried out with denaturation at 95°C for 15 sec, then at annealing temperature 52°C for 1min. After amplification, a melting curve was generated by heating the samples to 95°C for 15 sec, followed by cooling to 65°C for 20 sec and heating to 95°C for 15 sec. Fluorescence data were acquired during annealing or extension for reactions containing SYBR Green I. RT-minus products with all the reaction components except for the reverse transcriptase were produced for each sample, and were then employed for real-time PCR in order to demonstrate that the template for the PCR product was cDNA, not genomic DNA. The RT-minus control from the previous step and minus-template PCR control were included in each reaction of real-time PCR as negative controls. The minus-template PCR should have all the PCR components, with water substituted for the RT reaction aliquot, thus verifying that none of the PCR reagents are contaminated with DNA.

To construct the standard curve, the PCR product was purified after PCR and directly cloned into pMD 18-T vector (Takara, Number: D504A) according to the manufacturer's instructions. The plasmid DNA with the target sequence was purified with the help of the Tiangen Plasmid Maxi Kit (Tiangen, Beijing, China). pMD18T-MAD2 and pMD18T-β-actin used to generate the standard curve were amplified with the primers (Table 1) for real-time PCR. The concentrations of plasmid were evaluated by measuring the absorbance at 260 nm and expressed in a copy number of target fragments per milliliter.

The corresponding real-time PCR efficiency (E) in the exponential phase was calculated using the Equation $E = 10^{-1/\text{slope}} - 1$, applied to a dilution series ranging from 0.20 pg to 50 ng cDNA in triplicate (17). MAD2 transcript level was quantified by normalization to the housekeeping gene β-actin according to the 2(−Delta C(T)) Method (Livak and Schmittgen, 2001). Data for group differences were presented as mean ± standard deviation (SD) values.

TABLE 3. Ct Value of MAD2 and β-Actin Gene Transcript as Determined by qPCR Analysis (means ± SD)

Group	β-actin	MAD2
Control siRNA	26.22 ± 0.376	22.81 ± 0.156
MAD2 si RNA	27.29 ± 0.198	36.82 ± 0.085

Nuclear Examination of Oocytes

For examination of nuclear status at various time points of culture, oocytes were incubated with live cell nucleic acid stain, syto-11 (Molecular Probes, Eugene, OR, 1:1,000) for 1 hr at room temperature. Nuclear stages were categorized as GV, prometaphase I (ProM-I), metaphase I (M-I), anaphase I (A-I), telophase I (T-I), and metaphase II (M-II). Then the eggs were mounted on glass slides and examined with a TCS-4D laser scanning confocal microscope (Leica Microsystems, Bensheim, Germany). Nuclear stages were categorized as GV, prometaphase I (ProM-I), metaphase I (M-I), anaphase I (A-I), telophase I (T-I), and metaphase II (M-II).

Quantitation of Mad2 Gene Expression by Real-Time PCR

We can examine the oocytes morphologically for the presence of GV and PB1 with a StereoZoom microscope. GV oocytes were collected at 0 hr of culture; PreMI and MI oocytes were collected at 4 hr and 8 hr, respectively (excluding the GV oocytes); MII oocytes were collected at 12 hr as judged by the presence of PB1. MAD2 mRNA downregulation level was conducted using oocytes 0 hr after transfection (7 hr after transfection). RNA isolation and Quantity RT-PCR were conducted using the methods mentioned above.

Confocal Microscopy

Immunofluorescent staining of MAD2, microtubules, and nuclei was based on the procedures reported previously (Zhang et al., 2004) with minor modifications. For microtubule and nucleus staining, after removal of zona pellucida (ZP) in acid Tyrode's solution (pH 2.5), oocytes were fixed in 4% paraformaldehyde in PBS for 30 min and then incubated in incubation buffer (0.5% Triton X-100 in 20 mM Hepes pH 7.4, 3 mM $MgCl_2$, 50 mM NaCl, 300 mM Sucrose, and 0.02% NaN_3) for 30 min. After washed in PBS containing 0.1% Tween 20 and 0.01% Triton X-100 three times and then blocked in 1 mg/ml bovine serum albumin (BSA) in PBS for 1 hr, the oocytes were incubated with 1:100 FITC-conjugated antibody. After another three washes, the oocytes were stained with 10 mg/ml propidium iodide (PI) for 10 min. For MAD2 and nucleus staining, the oocytes were incubated with MAD2 polyclonal antibody diluted 1:100 in PBS containing 1 mg/ml BSA at 4°C overnight. After another three washes, the oocytes were stained with 10 mg/ml propidium iodide (PI) for 10 min. Finally, the eggs were mounted on glass slides and examined with a TCS-4D laser scanning confocal microscope (Leica Microsystems, Bensheim, Germany).

TUNEL Reaction for Analysis of Oocyte Apoptosis

At 0 hr after transfection, all the oocytes at two groups were collected for TUNEL reaction. TUNEL reaction was carried out according to the manufacturer's protocol (Dingguo Biotechnology Co., Beijing, China), that is, oocytes were fixed in 4% formaldehyde for 0.5 hr at room temperature (RT). After fixation, the oocytes were washed with PBS and treated with 0.3% H_2O_2 for 30 min at RT. This was followed by washing twice and permeabilization in 0.1% Triton X-100 for 2 min on the ice. The oocytes were then washed twice in PBS and incubated with terminal deoxynucleotidyl transferase enzyme in the dark for 1 hr at 37°C. This was followed by two washes in buffer A and blocked in 3% BSA for 30 min at RT, then incubated in reaction buffer for 30–60 min and reaction solution for 20 min in the dark. After being stained with 0.5% Methyl green for 20 sec, oocytes were washed in PBS and examined under a microscope.

Statistical Analysis

All experiments were repeated at least three times. Excel (Microsoft) was used to analyze the data from all experiments. Significant differences were determined using Tukey multiple range test and $P < 0.05$ was considered significant.

RESULTS

Nuclear Maturation of Mouse Oocytes in Culture

At 0 hr of culture, most oocytes (580/618, 93.85%) were at the GV stage. By 4 hr of culture, 78.77% (523/664) of the oocytes underwent GVBD and proceeded to the ProM-I stage. The proportion of oocytes at the M-I stage was 83.55% (325/389) when examined at 8 hr. When the oocytes were cultured for 12 hr, 70% (252/360) reached the M-II stage. Some oocytes were still at the GV stage (36/360, 10%) and M-I stage (67/360, 18.61%) at 12 hr after culture. Typical images of oocyte maturation are shown in Figure 1.

Two-Step Real-Time PCR Using Fluoresence Dye Sybr Green

We have successfully amplificated 422 bp mouse MAD2 and 83 bp β-actin gene (Fig. 2) and obtained two plasmids (Figs. 3 and 4). The standard curves were generated from at least five points (Figs. 5c,6c). Individual experiment was repeated at least three times to evaluate the degree of variation. The threshold values of the triplicate standard samples were very consistent both within the same reaction and between identical experiments. The correlation coefficients of mouse MAD2 (Fig. 5c) and β-actin (Fig. 6c) gene were 0.99 and 0.993, respectively. The amplification efficiency of mouse MAD2 and β-actin gene were all near 100% based on formula $E = 10^{-1/S} - 1$. Our results demonstrate a valid approach for quantitative analysis of MAD2 mRNA.

Quantitative analysis of MAD2 mRNA level in GV, Pro M-I, MI, and MII stage oocytes was conducted and the results were presented in Table 2. We showed that MAD2 mRNA level was dramatically upregulated during mouse oocyte meiotic maturation. We showed that GV stage MAD2 mRNA level was obviously different from other three stages, while there was no dramatical change of MAD2 mRNA level among Pro M-I, MI, and MII stage oocytes.

Results from quantitative analysis of MAD2 mRNA in MAD2 siRNA and control siRNA treatment groups were presented in Table 3. Quantitative analysis showed that MAD2 transcript in mouse oocytes was dramatically downregulated after MAD2 siRNA treatment, and we did not observe statistically significant changes in Ct for β-actin. When using $2^{-\Delta\Delta CT}$ Method to analyze real-time quantitative data, we found that MAD2 transcript level was downregulated by more than 90%.

Confocal Microscopy of Protein Expression

The MAD2 siRNA experiment was complemented by MAD2 staining. The experiments were repeated three times. As expected, 55.7% (N = 192) of the MAD2 siRNA transfected oocytes failed to stain Mad2 0 hr after transfection (7 hr from the initiation of transfection), and the MAD2-negative percentage increased up to 81% (N = 178) and 92.9% (N = 211) at 10 hr and 20 hr after transfection. Whereas in control siRNA treatment group, consistent results (95.7%, N = 138; 94.3%,

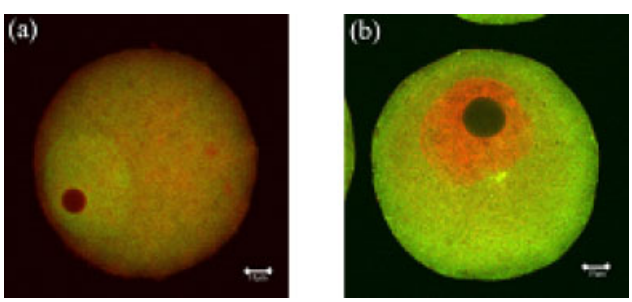

Fig. 7. Typical images of oocytes with positive (**a**) and negative (**b**) MAD2 protein signals. [See color version online at www.interscience.wiley.com.]

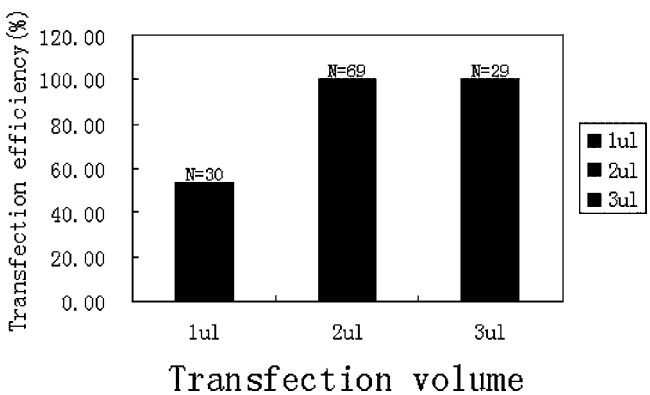

Fig. 8. Transfection optimization.

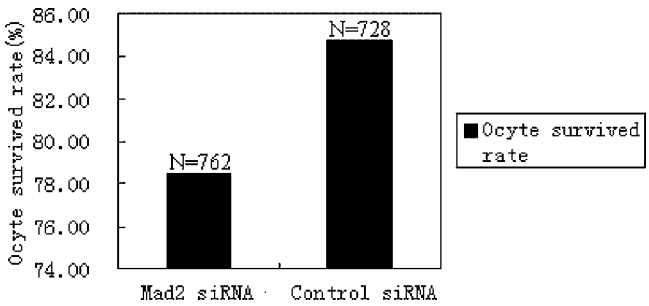

Fig. 9. Mouse oocytes survived after MAD2 siRNA and control siRNA treatment.

N = 158 and 93.2% N = 146) were obtained at different time points. MAD2 staining was present around in GV. Typical images of oocytes with positive signal and negative signal were shown in Figure 7.

Effect of siMad2 on Mouse Oocyte Meiotic Maturation

Using fluorescein conjugate control siRNA (Code sc-36869), 2 μl of 10 μM MAD2 siRNA is proper (Fig. 8). We also observed that after transfection, more oocytes died in MAD2 siRNA group than in control siRNA group (Fig. 9).

Having established the successful depletion of the MAD2 mRNA, we further examined its effect on mouse oocyte meiotic maturation. At 2, 4, and 6 hr after transfection, the oocyte GVBD ratio of MAD2 siRNA group and control siRNA group was 7.28% (n = 742) versus 46.05% (n = 773) ($P < 0.01$), 16.31% (n = 742) versus 55.11% (n = 773) ($P < 0.01$), 17.65% (n = 742) versus 56.27% (n = 773) ($P < 0.01$) (Fig. 10).

At 10 hr after transfection, the MII oocytes rates of MAD2 siRNA group and control siRNA group were 45.27% (n = 148) versus 17.52% (n = 274) ($P < 0.01$) (Fig. 11).

Effect of MAD2 siRNA Transfection on Spindle Apparatus Assembly

We observed that 8 hr after transfection MAD2 siRNA-treated oocytes had a higher percentage of spindle abnormity than control siRNA group (Fig. 12).

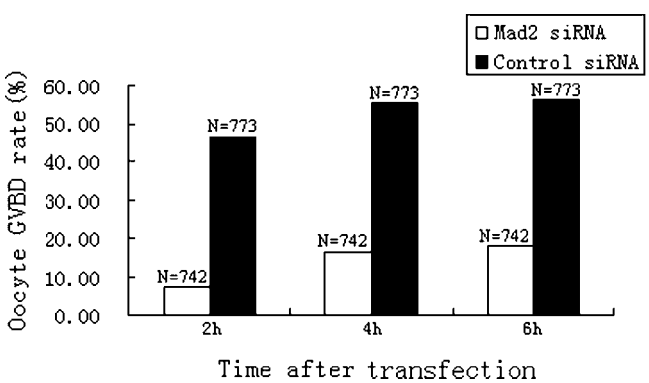

Fig. 10. Effect of MAD2 downregulation on mouse oocytes GVBD.

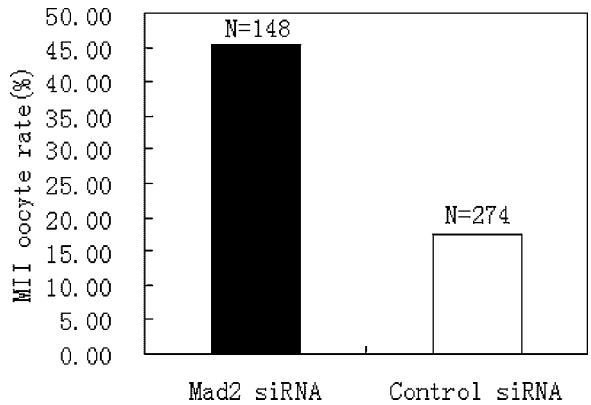

Fig. 11. MAD2 downregulation on mouse oocyte maturation progression.

Typical normal and abnormal spindle images were presented in Figure 13. A higher percentage of abnormal spindle organization was also observed in MAD2 siRNA-treated mature oocytes than in control siRNA group (Figs. 14,15).

MAD2 downregulation caused more oocytes to go apoptosis. We evaluated the oocyte apoptosis in Mad2 siRNA group and control siRNA group. By using the TUNEL reaction, Mad2 siRNA significantly increased oocyte apoptosis (Table 4). In the apoptotic oocytes, a great many dark-purple particles appeared around the GV (Fig. 16).

DISCUSSION

Quantitative real-time PCR, which includes absolute and relative quantification, is one of the most commonly used methods for analyzing gene expression. Here we used relative quantification method, and our PCR products were identified by generating a melting curve. We used $2^{-\Delta\Delta CT}$ method to analyze the data since it is a convenient way to analyze the relative changes in gene expression (Livak and Schmittgen, 2001).

RNA interference (RNAi) is one of the most exciting discoveries of the past decade in functional genomics

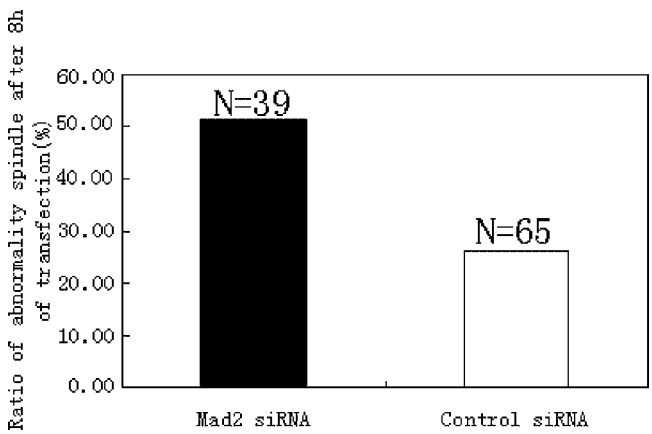

Fig. 12. Effect of MAD2 downregulation on spindle morphology of mouse oocytes (8 hr after transfection).

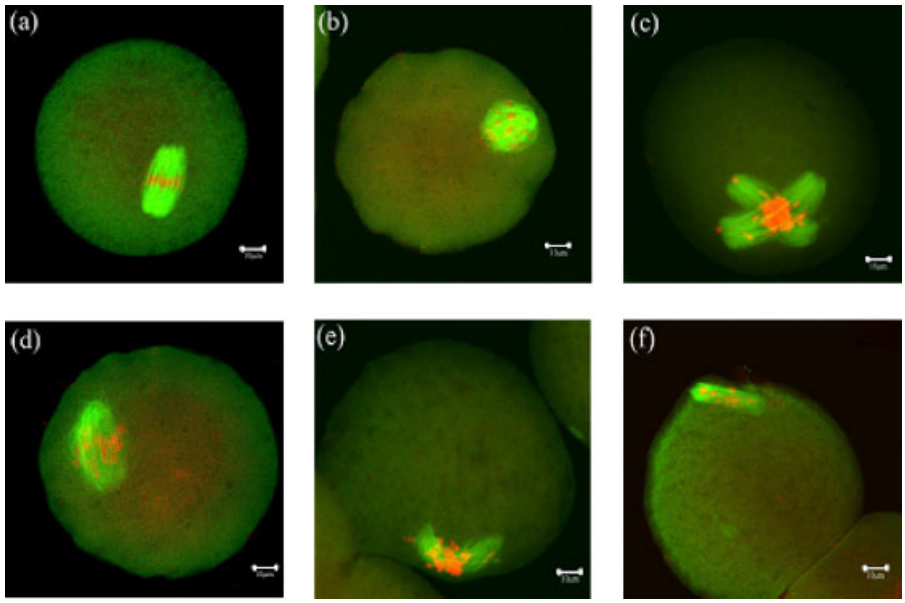

Fig. 13. Normal and abnormal spindle images observed at 8 hr after transfection. **a**: normal image. **b**–**f**: abnormal images. [See color version online at www.interscience.wiley.com.]

and proteomics. RNA interference is rapidly becoming a useful research tool for gene silencing. Although people reported previously that quantitative analysis of MAD2 transcripts in human oocytes is relatively stable (Steuerwald et al., 2001), using MAD2 siRNA transfection, we showed that MAD2 mRNA level was dramatically upregulated during mouse oocyte meiotic maturation. We showed that during mouse oocyte meiotic maturation GV stage MAD2 mRNA level was obviously different from other three stages, while there was no dramatical change of MAD2 mRNA level among pro M-I, MI, and MII stage oocytes. Using MAD2 siRNA transfection, we have successfully decreased MAD2 transcript and protein expression in mouse oocytes. As a member of spindle checkpoint proteins and part of the mitotic checkpoint complex (MCC), MAD2 takes a central role in the regulation of anaphase onset and genome integrity. Previous studies on MAD2 downregulation by small MAD2 mRNA injection showed that the meiotic cell cycle was shortened, and oocyte aneuploidy was increased (Michel et al., 2001, 2004; Homer et al., 2005b). By using this siRNA transfection approach, we demonstrated that MAD2 downregulation resulted in a decrease in GVBD rate, a shortened duration of meiosis I, and meiotic apparatus abnormality. Based on our results, MAD2 protein downregulation interrupted the correct chromosome alignment on the spindle, and caused the early entry to anaphase before all the chromosomes well attached to the MI spindle microtubules. Even in mature MAD2 siRNA transfected oocytes, a high proportion of oocytes did not show normal chromosome alignment. Our results provide further evidence for the role of MAD2 as a meiotic spindle checkpoint protein in mouse oocytes. In addition, we found that MAD2 siRNA transfection decreased GVBD rate of oocytes. Whether this is caused by transfection manipulation or by MAD2 downregulation is not clear.

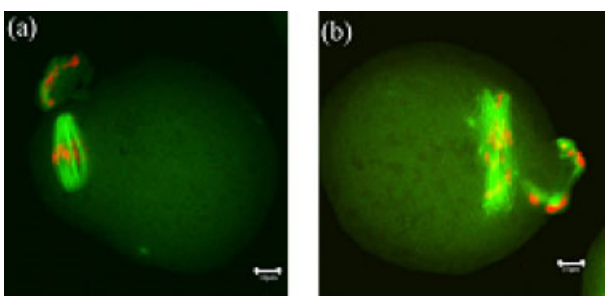

Fig. 14. Normal and abnormal spindle images in siRNA-treated mature oocytes. **a**: normal image. **b**: abnormal image. [See color version online at www.interscience.wiley.com.]

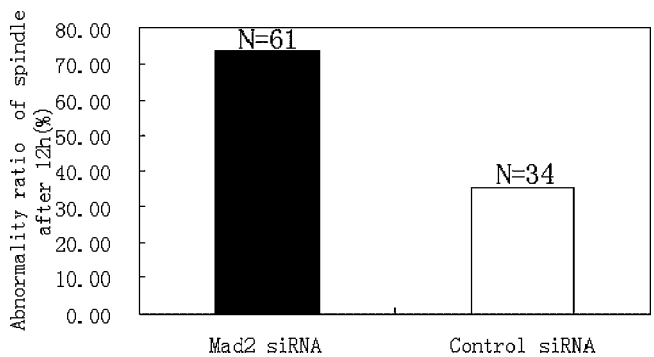

Fig. 15. Effect of MAD2 downregulation on spindle morphology of mouse mature oocytes (12 hr after transfection).

TABLE 4. Apoptosis in MAD2 RNAi Mouse Oocytes

Group	No. of oocytes examined[a]	No. of apoptosis(%)
Control siRNA	224	0[b]
MAD2 siRNA	324	65(20.06 ± 3.6)[c]

[a]Experiments were repeated three times.
[b]versus [c], significantly different, $P < 0.01$.

We also showed that Mad2 siRNA transfection caused 1/5 oocytes to go apoptosis (Table 4). We identified apoptosis by the TUNEL reaction. Our recent study showed that aging of oocytes reduced expression in spindle checkpoint protein and anti-apoptosis protein in pig oocytes. These events in turn cause abnormal sister chromatid segregation and apoptosis (Ma et al., 2005). Dobles et al. (2000) and Yin et al. (2006) hold identical views. Dobles et al. (2000) knocked out Mad2 in mice embryonic cells and found widespread chromosome missegregation and apoptosis. Yin et al. (2006) found that SGC7901 cells overexpressing Mad2 beta variant decreased the relative expression of efficient MAD2 and became more resistant to adriamycin, vincristine, and mitomycin by abrogating mitotic arrest and apoptosis. Whereas Cheung et al. (2005) pointed out that the MAD2-induced chemosensitization to cisplatin in NPC cells was mediated through the induction of mitotic arrest, which in turn activates the apoptosis pathway. In our view, these results are not conflict with each other, since both MAD2 downregulation and overexpression disturb the normal mitotic or meiotic cycle and could induce apoptosis.

In conclusion, our study shows that siRNA transfection is an effective approach to study MAD2 function, and our results provide further evidence for the role of MAD2 as a spindle checkpoint protein in mouse oocytes.

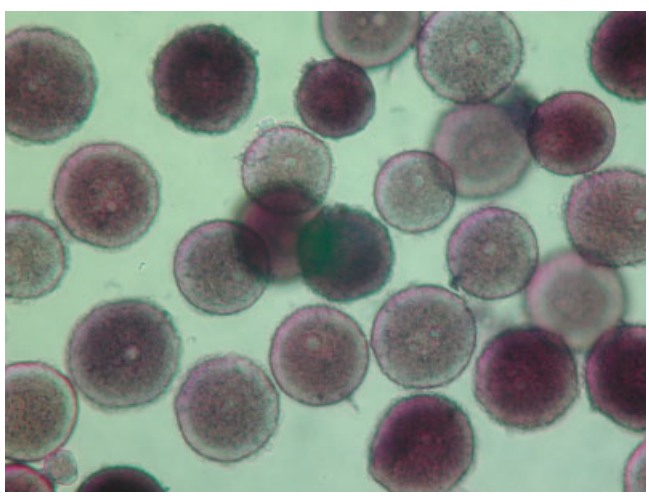

Fig. 16. Images of apoptotic oocytes detected by TUNEL reaction. A great many dark-purple particles appeared in the cytoplasm of apoptotic oocytes. [See color version online at www.interscience.wiley.com.]

ACKNOWLEDGMENTS

We thank S. Taylor for his gifts of MAD2 antibody reagents.

REFERENCES

Bharadwaj R, Yu H. 2004. The spindle checkpoint, aneuploidy, and cancer. Oncogene 23:2016–2027.

Cheung HW, Jin DY, Ling MT, Wong YC, Wang Q, Tsao SW, Wang X. 2005. Mitotic arrest deficient 2 expression induces chemosensitization to a DNA-damaging agent, cisplatin, in nasopharyngeal carcinoma cells. Cancer Res 65:1450–1458.

Dobles M, Liberal V, Scott ML, Benezra R, Sorger PK. 2000. Chromosome missegregation and apoptosis in mice lacking the mitotic checkpoint protein Mad2. Cell 101:635–645.

Homer HA, McDougall A, Levasseur M, Murdoch AP, Herbert M. 2005a. Mad2 is required for inhibiting securin and cyclin B degradation following spindle depolymerisation in meiosis I mouse oocytes. Reproduction 130:829–843.

Homer HA, McDougall A, Levasseur M, Yallop K, Murdoch AP, Herbert M. 2005b. Mad2 prevents aneuploidy and premature proteolysis of cyclin B and securin during meiosis I in mouse oocytes. Genes Dev 19:202–207.

Lazar S, Gershon E, Dekel N. 2004. Selective degradation of cyclin B1 mRNA in rat oocytes by RNA interference (RNAi). J Mol Endocrinol 33:73–85.

Livak KJ, Schmittgen TD. 2001. Analysis of relative gene expression data using real-time quantitative PCR and the 2(-Delta Delta C(T)) Method. Methods 25:402–408.

Ma W, Zhang D, Hou Y, Li YH, Sun QY, Sun XF, Wang WH. 2005. Reduced expression of MAD2, BCL2, and MAP kinase activity in pig oocytes after in vitro aging are associated with defects in sister chromatid segregation during meiosis II and embryo fragmentation after activation. Biol Reprod 72:373–383.

Michel LS, Liberal V, Chatterjee A, Kirchwegger R, Pasche B, Gerald W, Dobles M, Sorger PK, Murty VV, Benezra R. 2001. MAD2 haploinsufficiency causes premature anaphase and chromosome instability in mammalian cells. Nature 409:355–359.

Michel L, Benezra R, Diaz-Rodriguez E. 2004. MAD2 dependent mitotic checkpoint defects in tumorigenesis and tumor cell death: A double-edged sword. Cell Cycle 3:990–992.

Musacchio A, Hardwick KG. 2002. The spindle checkpoint: Structural insights into dynamic signalling. Nat Rev Mol Cell Biol 3:731–741.

Steuerwald N, Cohen J, Herrera RJ, Sandalinas M, Brenner CA. 2001. Association between spindle assembly checkpoint expression and maternal age in human oocytes. Mol Hum Reprod 7:49–55.

Wang WH, Sun QY. 2006. Meiotic spindle, spindle checkpoint and embryonic aneuploidy. Front Biosci 11:620–636.

Wassmann K, Niault T, Maro B. 2003. Metaphase I arrest upon activation of the Mad2-dependent spindle checkpoint in mouse oocytes. Curr Biol 13:1596–1608.

Yin F, Du Y, Hu W, Qiao T, Ding J, Wu K, Liu Z, Fan D. 2006. Mad2beta, an alternative variant of Mad2 reducing mitotic arrest and apoptosis induced by adriamycin in gastric cancer cells. Life Sci 78:1277–1286.

Zhang D, Ma W, Li YH, Hou Y, Li SW, Meng XQ, Sun XF, Sun QY, Wang WH. 2004. Intra-oocyte localization of MAD2 and its relationship with kinetochores, microtubules, and chromosomes in rat oocytes during meiosis. Biol Reprod 71:740–748.